Approximate Bisimulations for Sodium-Channel Dynamics

Abhishek Murthy[1], Ariful Islam[1], Ezio Bartocci[2], Elizabeth Cherry[3], Flavio H. Fenton[3], James Glimm[4], Scott A. Smolka[1], and Radu Grosu[2]

[1] Department of Computer Science, Stony Brook University
[2] Department of Computer Engineering, Vienna University of Technology
[3] Department of Biomedical Sciences, Cornell University
[4] Department of Applied Mathematics and Statistics, Stony Brook University

Abstract. This paper shows that, in the context of the Iyer et al. 67-variable cardiac myocycte model (IMW), it is possible to replace the detailed 13-state continuous-time MDP model of the sodium-channel dynamics, with a much simpler Hodgkin-Huxley (HH)-like two-state sodium-channel model, while only incurring a bounded approximation error. The technical basis for this result is the construction of an *approximate bisimulation* between the HH and IMW channel models, both of which are input-controlled (voltage in this case) continuous-time Markov chains. The construction of the appropriate approximate bisimulation, as well as the overall result regarding the behavior of this modified IMW model, involves: (1) The identification of the voltage-dependent parameters of the m and h gates in the HH-type channel, based on the observations of the IMW channel. (2) Proving that the distance between observations of the two channels never exceeds a given error. (3) Exploring the sensitivity of the overall IMW model to the HH-type sodium-channel approximation. Our extensive simulation results experimentally validate our findings, for varying IMW-type input stimuli.

1 Introduction

The emergence of high-throughput data-acquisition equipment has changed cell biology, from a purely wet-lab-based science to also an engineering and information science. The identification of a mathematical model from cellular experimental data, and the use of this model to predict and control the cell's behavior, are nowadays indispensable tools in cell biology's arsenal [35, 5].

Continual progress in data-acquisition has also led to the creation of increasingly-sophisticated partial Differential Equations Models (DEMs) for cardiac cells (myocytes). These are similar in spirit to the DEMs used in physics: their main purpose is to elucidate the biological laws governing the electric behavior of cardiac myocytes, i.e., their underlying cellular and ionic processes [9].

Inspired by the squid-neuron DEM [20] developed by Hodgkin and Huxley (HH), Luo and Rudy (LR) devised one of the first myocyte DEMs, for guinea-pig ventricular cells [29]. Adapting this model to human myocytes led to the

Tusscher-Noble^2-Panfilov (TNNP) DEM [40], which has 17 state variables and 44 parameters. Based on more recent experimental data, Iyer, Mazhari and Winslow (IMW) subsequently developed a DEM comprising 67 state variables and 94 parameters [21]. This DEM reflects the state-of-the-art understanding of biological entities regulating the electric behavior of human myocytes.

From 17 to 67 variables, all such DEMs capture myocytic behavior at a particular level of abstraction, and hence all of them play an important role in the modeling hierarchy. It is essential, however, to maintain focus on the purpose of a particular DEM; that is, of the particular cellular and ionic processes whose behavior the DEM is intended to capture. Disregarding this purpose may lead to the use of unnecessarily complex DEMs, which may render not only analysis, but also simulation, intractable.

If the only entity-of-interest is the myocyte's transmembrane voltage, co-authors Cherry and Fenton have experimentally shown that a minimal DEM (MM) consisting of only 4 variables and 27 parameters, can accurately capture voltage-propagation properties in 1D, 2D, and 3D networks of myocytes [4]. This MM has allowed us to obtain dramatic simulation speedups [1], and to use its linear hybridization as the basis for formal symbolic analysis [19].

Since new technological advances are expected to lead to further insights into myocytic behavior, it is likely that IMW will be further refined, by adding new variables. As in model checking and controller synthesis, one would therefore like to compute the smallest approximation of the State-Of-the-Art DEM (SOA), which is observationally equivalent to the SOA for the property of interest, modulo some specified approximation error. This, however, is not an easy task, as it implies the automatic approximation of very large nonlinear DEMs.

A first step towards the desired automation is to identify a set of approximation techniques that allow one to systematically remove unobservable variables from, say, the SOA to end up with the MM, if the only observable variable is the voltage. This is one of the goals of our work within the CMACS project [36]. A byproduct of this work is to establish a long-missing formal relation among the existing myocyte-DEMs, facilitating the transfer of properties established at one layer of abstraction to the other layers. The use of such *Towers of abstraction* is becoming an increasingly prevalent in systems biology [23, 11].

The main focus of this paper is on *sodium-channel approximations*. In the HH DEM and the DEM of Noble [37], the sodium channel is assumed to consist of four independent Markovian gates, whose opening and closing rates depend on the transmembrane voltage. Three of the gates are identical activation gates m, and the fourth is an inactivation gate h. The sodium channel is conducting if all of four gates are in the open state.

Based on the work of Beeler and Reuter [3], TNNP refines the inactivation gate h into two independent inactivation gates, a fast one, still labeled as h, and a slow one, labeled as j. Hence, the encoding of the sodium channel requires in the above DEMs two and respectively three (gating) variables. IMW, however, uses the formulation of Irvine [28], where new experimental data is used to show that

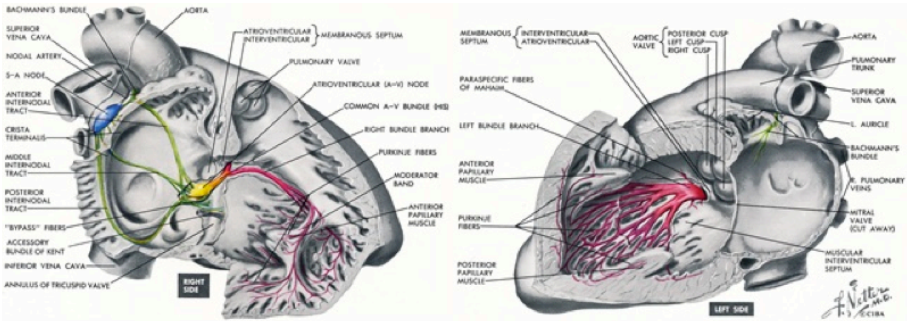

Fig. 1. Conduction system of the human heart ((Illustration taken from F. H. Netter, The CIBA Collection of Medical Illustrations. Vol. 5 Heart. CIBA Pharmaceutical Comp., New York, 1978).

the five gates are interdependent. This leads to a considerably larger Markovian model for the sodium channel, consisting of 13 state variables.

The main question posed in this paper is the following: *assuming that conductance of the sodium channel is the only observable, is the behavior of the HH channel equivalent to the behavior of the IMW channel, modulo a well defined approximation error?* More technically, is it possible to construct an approximate bisimulation [12, 14, 13, 15] between the HH-channel and IMW-channel models?

The answer to this question is of broad interest, as it reduces to showing the existence of an approximate bisimulation between two continuous-time Markov decision processes (CT-MDPs), that is, two input-controlled (voltage in this case) continuous-time Markov chains (CTMCs). We answer this question in the positive, by explicitly constructing such a bisimulation.

The construction involves: (1) The identification of the voltage-dependent parameters of the m and h gates in the HH-type channel, based on the observations of the IMW channel. (2) Proving that the distance between the observations of the two channels never exceeds a given error. (3) Exploring the sensitivity of the overall IMW DEM to the HH-type sodium-channel approximation.

The rest of the paper is organized as follows. Section 2 introduces the relevant background for the HH and the IMW DEMs and their sodium-channel MDP formulations. Section 3 presents our parameter-identification technique and the resulting HH-type MDP for the sodium channel. Section 4 proves the existence of an approximate bisimulation between the HH and IMW sodium-channel MDPs. Sections 5 and 6 discuss related work, our conclusions, and future directions.

2 Background

The heart, see Fig. 1, is the central organ of the circulatory system, responsible for pumping blood in the pulmonary and systemic circulation loops [8]. Pumping is achieved through the synchronized contraction of around four billion myocytes. This is controlled in a distributed fashion, through the propagation and reinforcement of an electric pulse (clock). The pulse originates in the sino-atrial node of

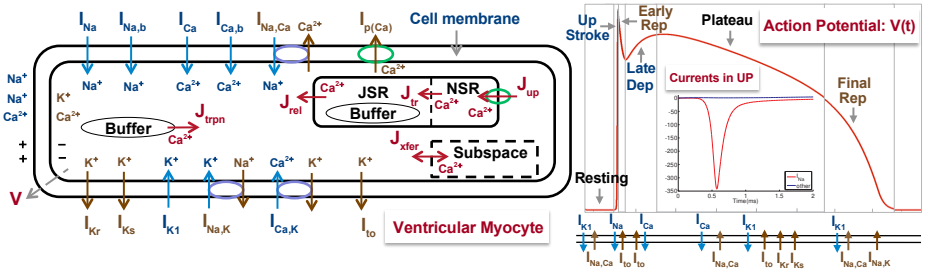

Fig. 2. (Left) Currents in IMW: Blue and brown arrows show ionic currents flowing through channels. Blue circles and arrows correspond to ionic exchanger currents and green circles denote ionic pumps. Intra-cellular currents are shown in Magenta. (Right) The action potential (AP), its phases and associated currents. (Right-Inlay) Sodium current in red, and the sum of all other currents in blue, in upstroke phase (UP).

the heart, and diffuses from myoucyte to myocyte, through a very sophisticated communication inftrastructure, arranged into various sheets and fibers.

Myocytes belong to the class of excitable cells (EC), which also includes neurons, and muscle cells. An EC has electrochemical excitability-properties, responsible for the conduction and reinforcement of the electric pulse known as the action potential (AP). The shape of a typical myocyte AP and its associated phases are shown in Fig. 2(Right). While at rest, an EC polls the AP diffused from its neighbouring cells: If the AP is above of a certain threshold, then the EC's membrane goes through a depolarization and a repolarization sequence, which results in the reinforcement of the AP. In this paper, we will be mainly concerned with the first depolarization phase, known as the the upstroke.

2.1 The IMW Cellular Model

The IMW DEM is the SOA electric model capturing the ionic processes responsible for the generation of an AP in human ventricular myocytes:

$$-C\dot{V}=I_{Na}+I_{Na_b}+I_{Ca}+I_{Ca_b}+I_{K_r}+I_{K_s}+I_{K_1}+I_{to_1}+I_{p(Ca)}+I_{NaCa}+I_{NaK}+I_{CaK}+I_{st} \quad (1)$$

where, V is the membrane's potential, $\dot{V}$ is its first-order time derivative, C is the membrane's capacitance, and I_v are the ionic currents shown in Fig. 2(Left), except for I_{st}. This is the stimulus current, which could be either an external stimulus or the diffused charge from neighboring cells.

The remaining currents are the result of the flow of the sodium Na^+, potassium K^+ and calcium Ca^{2+} ions, respectively, across the myocyte's membrane. Three transport mechanisms are responsible for the ion flows: ion channels, ion pumps and ion exchangers. Channels are special proteins that penetrate the membrane's lipid bi-layer, and which are selectively permeable to ions. Depending on the conformation of the constituent-protein, the channel either allows or does not allow, an unidirectional movement of certain ion species.

The protein conformation is voltage dependent, thus the name voltage-gated channels. All the transmembrane currents in Fig. 2 result from voltage-gated

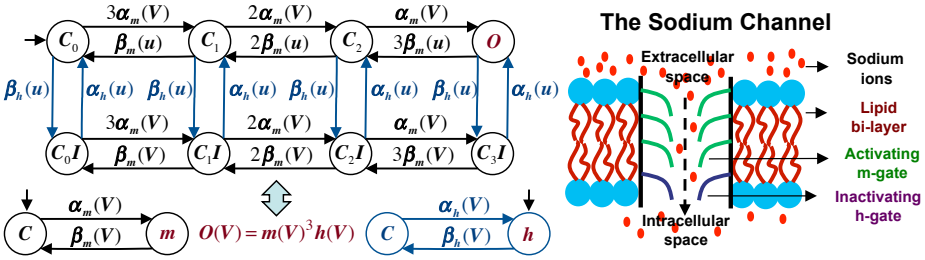

Fig. 3. (Left-top) Sodium channel MDP in 8 states counting the number of indpendent open/closed gates, and observation function $O(t)$. (Left-bottom) The open-closed MDPs for the $m(V)$ and $h(V)$ gates. The equivalent sodium channel behavior is obtained as $O(t) = m(V)^3 h(V)$. (Right) The schematic representation of the sodium channel with its associated independent gates.

ionic channels, except for I_{NaK}, I_{NaCa}, I_{CaK} and $I_{p(Ca)}$, which are exchanger- or pump-currents. The concentration of the calcium is regulated by a sophisticated intracellular mechanism, which is not important for purpose of this paper.

Fig. 2(Right-inlay) plots the sodium current I_{Na} and the sum of all other ionic currents during the upstroke phase (UP), of a typical AP of the IMW DEM. The sodium current I_{Na} dominates all the other. *The opening of the sodium channel, which causes the flow of I_{Na}, chiefly contributes to the upstroke phase, and will be the focus of the remainder of the paper.* In HH the situation is similar, and in MM the role of I_{Na} is played by an abstract fast inward current J_{fi}.

2.2 The HH Sodium Current

The sodium current I_{Na} in the HH DEM is defined by the following equation:

$$I_{Na} = \overline{g}_{Na}\, m^3(V)\, h(V)\, (V - V_{Na})$$

where $\overline{g}$ is the maximum conductance of the sodium channel, V_{Na} is the sodium's channel Nernst potential, $m(V)$ is the voltage-dependent activation gate, and $h(V)$ is the voltage-dependent inactivation gate.

A graphic illustration of the sodium channel is given in Fig. 3 (Right). It consists of four independent voltage-controlled gates, three of which are identical activation gates $m(V)$, and one of which is an inactivation gate $h(V)$.

The activation and inactivation gates are shown in Fig. 3 (Left-bottom). They are continuous-time Markov decision processes (CT-MDP). Both CT-MDPs have a closed and an open state, respectively, and the rate of transitioning between these two states is given by the voltage-dependent parameters $\alpha(V)$ and $\beta(V)$. At rest the m-gate is closed and the h-gate is open. Their DEM is as follows:

$$\dot{m} = \alpha_m(V)(1 - m) - \beta_m(V)m, \qquad \dot{h} = \alpha_h(V)(1 - h) - \beta_h(V)h$$

We refer to this DEM as M_H. The linear system obtained by fixing $V = v$ will be denoted ad M_H^v. The observation function O of this DEM is given by

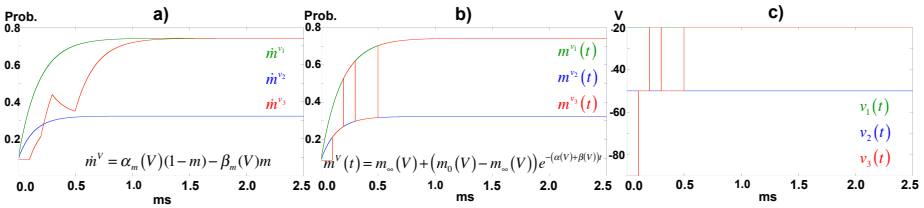

Fig. 4. Probability for the m-gate to be open in HH: a) Numerical integration of m for different voltage changes; b) Analytical solution of m for different voltage changes; c) Voltage changes applied for the analytical and the numerical integration solutions.

$m(V)^3h(V)$, which is the result of independence among the gates. Introduce now the following notation:

$$x = [m, h]', \quad A = diag(-(\alpha_m + \beta_m), -(\alpha_h + \beta_h)), \quad B = [\alpha_m, \alpha_h]'$$

The independence of the gates also implies that the DEM is in diagonal form, and it can be therefore written as follows:

$$\dot{x} = Ax + B, \qquad x_0 = [m_0, h_0]'$$

Despite of the linear-looking form, this equation is nonlinear, as A and B depend on the voltage. For example, Figure 4(a) shows its numeric solution for the input in Figure 4(c). However, HH computed an approximate closed form solution as follows. In the resting state, defined as $V = 0$, and in the equilibrium state, for a fixed $V = v$, the gates m and h, and the rates τ have the following values:

$$\begin{array}{ll} m_0 = \alpha_{m_0}/(\alpha_{m_0} + \beta_{m_0}), & m_\infty = \alpha_m/(\alpha_m + \beta_m) \\ h_0 = \alpha_{h_0}/(\alpha_{h_0} + \beta_{h_0}), & h_\infty = \alpha_h/(\alpha_h + \beta_h) \\ \tau_m = 1/(\alpha_m + \beta_m), & \tau_h = 1/(\alpha_h + \beta_h) \end{array}$$

Then solving the DEM above as if A and B were constant and the differential equation therefore linear, Hodgkin and Huxley derived the following solution:

$$x = [m_\infty - (m_\infty - m_0)e^{-t/\tau_m}, h_\infty - (h_\infty - h_0)e^{-t/\tau_h}]'$$

As shown in Figure 4(b) this closed-form solution jumps for a the changing input shown in Figure 4(c) between the solutions obtained for constant input. This behavior is however not problematic when replaced in the cellular model, as the voltage only jumps at the beginning, when the stimulus is applied, and then varies in a continuous way.

One can prove that the 7-state-variables MDP (the value of the 8th results from the stochasticity property) shown in Fig. 3(Left-top), counting the number of m and respectively h channels open, is an exact bisimulation of the MDP in two states. Define the state maps:

$$C_i = C_3^i(1-m)^{3-i}m^i h, \qquad C_i I = C_3^i(1-m)^{3-i}m^i(1-h)$$

Then taking as observation function O in the top MDP and the observation $O = m^3h$ in the bottom MDP, one cannot distinguish between the two.

2.3 The IMW Sodium Current

The sodium current I_{Na} in the IMW DEM is defined by the following equation:

$$I_{Na} = \overline{g}_{Na} \left(O_1(V) + O_2(V)\right) (V - V_{Na})$$

where $\overline{g}$ and V_{Na} have the same meaning as in the HH DEM, and $O_1(V)$ and $O_2(V)$ correspond to the probability of two states of the MDP shown in Fig. 5.

The SOA IMW view of the Sodium channel is shown Fig. 5[26, 28], with transition rates in Table 1. There are now four identical m gates, and the transition rates of the h gate are constant. However, these rates indirectly depend on V through the number of open-closed m gates (encoded as powers of a).

Moreover, taking the path C_0, C_1, C_1I, C_0I is mathematically equivalent to taking a voltage dependent h-transition C_0, C_0I. The longer the paths, the less one can distinguish between a HH-type and an IMW-type transition. This intuition is the basis for our bisimulation proof. Note also that two states O_1 and O_2 are now observable instead of one, and some bookeeping was also added.

Dependence and bookeeping are considerable obstacles for searching for a closed form solution of IMW, or a bisimulation state-map, similar to the one given previous section. We will therefore explicitly construct an HH abstraction, and associated approximate bisimulation from the runs of the IMW.

Definition 1. *Consider the 13-state model for sodium-channel dynamics shown in Fig. 5. Let p_j denote the j^{th} state-occupancy-probability from the vector $\mathbf{p} = (C_0, C_1, C_2, C_3, C_4, O_1, O_2, C_0I, C_1I, C_2I, C_3I, C_4I, I)$. The dynamics of the model is described by the system of differential equations M_I:*

$$\frac{dp_j}{dt} = \sum_{i \neq j} k_{ij}(V) p_i - \sum_{i \neq j} k_{ji}(V) p_j \qquad i, j = 1 \ldots 13 \tag{2}$$

where, V is the transmembrane potential and $k_{ij}(V)$ is the transition rate from the i^{th} to the j^{th} state as defined in Table 1. This system can be re-written as:

$$\frac{dp_j}{dt} = A(V).\mathbf{p} \tag{3}$$

where, $A(V)$ is a 13×13 matrix with $A_{j,i}(V) = k_{ij}(V)$ $i \neq j$, $A_{j,j}(V) = -\sum_{i \neq j} k_{ji}$. The linear system M_{I^v} is obtained from M_H by fixing $V = v$ in Eq. 3.

rate	function	rate	function	rate	function
$\alpha(V)$	$c.e^{-19.6759+0.0113V}$	$\delta\delta(V)$	$c.e^{-38.4839-0.1440V}$	ϵ	0.0227
$\beta(V)$	$c.e^{-26.2321-0.0901V}$	$\gamma\gamma(V)$	$c.e^{-21.9493+0.0301V}$	ω	1.0890
$\gamma(V)$	$c.e^{-16.5359+0.1097V}$	$\eta(V)$	$c.e^{-19.6729+0.0843V}$	c_n	0.7470
$\delta(V)$	$c.e^{-27.0926-0.0615V}$	$O_n(V)$	$c.e^{-20.6726+0.0114V}$	c_f	0.2261
$\nu(V)$	$c.e^{-26.3585-0.0678V}$	$O_f(V)$	$c.e^{-39.7449+0.0027V}$	a	1.4004

Table 1. Rates of the 13-state stochastic model for sodium channel dynamics in Fig. 5. $c = 8.513 \times 10^9$. Values instantiated from Table 6 of [21] at temperature T = 310K.

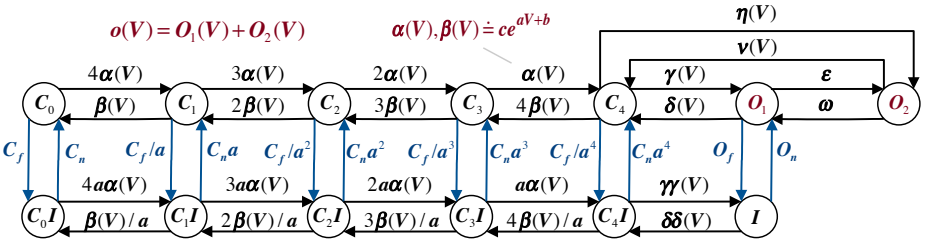

Fig. 5. The 12-state-variables MDP of the IMW model. The observation function is now $O = O1 + O_2$, and the transition rates of the h gate are constants. However, they depend through a on the number of m-gates open.

3 Abstraction of Sodium Channel Dynamics

We construct a HH-type DEM M_H that can substitute M_I within the IMW cardiac cell-model. We perform the following abstractions in this process:

- We reduce the number of activating subunits to 3 and use a single inactivating subunit. This results in abstracting away the I, C_3I, C_4I, C_3 and C_4I.
- We coalesce the two open states into a single open state O.
- We abstract away the conditional dependence between activating and inactivating subunits of the 13-state model M_I (difference **D2**). This is done by abstracting away the scaling factor a.
- With the above abstractions, M_I reduces to the 8-state stochastic model. The 8-state abstraction then reduces to the 2-state HH model due to the invariant manifold reduction.

Our approach to obtaining the 2-state HH-type abstraction from the 13-state stochastic model is summarized in Fig. 6 and described below.

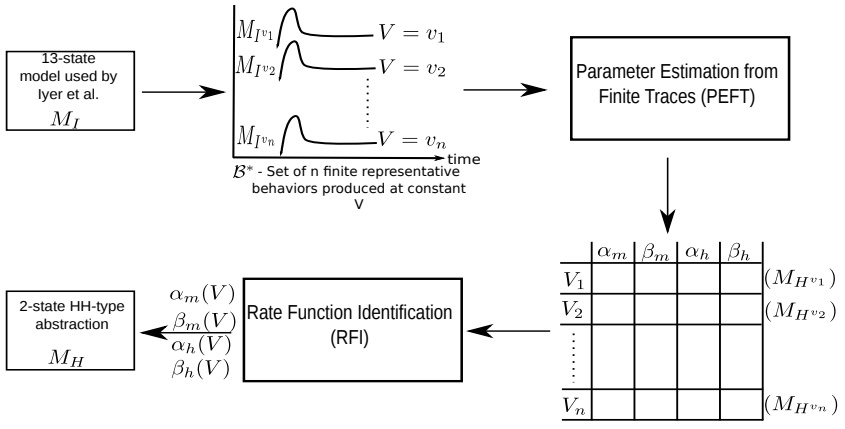

Fig. 6. Abstraction process for sodium-channel dynamics.

1. **Generating representative finite traces of M_I**
   The IMW model was simulated in FORTRAN for a single cell at a time scale of 10^{-4} ms. Multiple M_{I^v} systems were simulated for the values of V observed during the FORTRAN simulation. The linear system M_{I^v} was simulated in MATLAB using the *ODE45* solver [32]. The time scale for these simulations was 10^{-2} ms. The simulations ran till the steady state was reached. The initial condition for all the simulations were taken to be the initial condition specified in Table 4 of [21]. The motivation for these initial conditions lies in the voltage-clamp experiments performed in [20]. In these experiments, the voltage was initial maintained at the resting potential, with the neuron-conductance also being in the resting state. The voltage was suddenly increased to a specified value and the evolution of conductance was observed till steady state.
   The simulations resulted in a set $\mathcal{B}^*$, of finite-length representative behaviors (traces). Each member $\mathcal{B}^*(v)$ is the trajectory of the simulation of M_I^v.
2. **Parameter Estimation from Finite Traces (PEFT)**
   This routine takes $\mathcal{B}^*$ as the input and at each of the voltage-values v_i, estimates the parameters of $M_{H^{v_i}}$, the two-state HH model (M_H) at $V = v_i$. For each voltage v, the following optimization problem was solved to estimate the parameters α_m^v, β_m^v, α_h^v and β_h^v of M_{H^v}:

$$\begin{aligned} &\text{minimize} \sum_{t=0}^{t_S^v} [O^v(t) - m^v(t)^3 h^v(t)]^2 \\ &\text{subject to:} \quad \alpha_m^v, \beta_m^v, \alpha_h^v, \beta_h^v \geq 0 \end{aligned} \tag{4}$$

   where,
   - t is the discrete-time step.
   - t_S^v is the number of discrete-time steps taken by M_{I^v} to reach steady state (M_{I^v} was simulated in MATLAB till steady-state).
   - $O^v(t) = O_1^v(t) + O_2^v(t)$ is the sum of the occupancy probabilities of states O_1 and O_2 in the trajectory $\mathcal{B}^*(v)$.
   - $m^v(t)$, $h^v(t)$ define a trajectory of M_H^v. At fixed membrane potential $V = v$, $m^v(t)$ and $h^v(t)$ can be written in closed form as:

$$\begin{aligned} m^v(t) &= \frac{\alpha_m^v}{\alpha_m^v + \beta_m^v} + (m^v(0) - \frac{\alpha_m^v}{\alpha_m^v + \beta_m^v}) \exp(-(\alpha_m^v + \beta_m^v)t) \\ h^v(t) &= \frac{\alpha_h^v}{\alpha_h^v + \beta_h^v} + (h^v(0) - \frac{\alpha_h^v}{\alpha_h^v + \beta_h^v}) \exp(-(\alpha_h^v + \beta_h^v)t) \end{aligned} \tag{5}$$

     where, $m^v(0)$ and $h^v(0)$ denote initial conditions.

   We used MATLAB's constrained-optimization solver *FMINCON*[33] for Eq. (4). Details of the active-set optimization algorithm implemented in the function can be found in [30]. Three aspects of our implementation deserve further elaboration:
   - **Choosing $m^v(0)$ and $h^v(0)$** - In [20], the authors choose the initial conditions for all the voltages such that the inactivating-gating-variable h is high and the activating-gating-variable m is low. We use the same convention but ensure that the initial conductance (observation)

$m^v(0)^3 h^v(0) = O^{V_{res}}$, where $O^{V_{res}}$ is the conductance $O_1 + O_2$ of M_I at the resting potential V_{res}. Specifically, $m^v(0) = 0.0026$ and $h^v(0) = 0.95$ for all v.

- **Providing seed-values** - For each voltage-value v, FMINCON needs seed values of α_m^v, β_m^v, α_h^v and β_h^v to start optimizing over the parameter space. We implemented a local search strategy for this purpose. The parameters estimated at v_i were used as seed-values for v_{i+1}. For the resting potential, when $i = 1$, the seed values were taken by evaluating Eq. (16)-(18) of [37] at $V = -90.66mV$ (the resting potential).
- **Local minima** - The solver is guaranteed to provide parameter-values that locally minimize the objective function. FMINCON was run multiple times until the objective function was minimized to a value below a pre-defined threshold. The terminal values of an iteration were perturbed and used as seed-values for the next iteration. A maximum of 100 iterations were performed.

PEFT resulted a in a table of parameters θ, again indexed by voltage, i.e. θ^v contained the parameters of M_{H^v}.

3. **Rate-Function Identification (RFI)**
   RFI combines the parameters θ^v, of M_{H^v}, and outputs the parameter-functions of M_H, which are functions of V. This is done by identifying appropriate forms for the parameter functions $\alpha_m(V)$, $\beta_m(V)$, $\alpha_h(V)$ and $\beta_h(V)$ and then using MATLAB's curve-fitting toolbox [31] to estimate the parameters of the chosen form.

$$\alpha_m(V) = -0.6 + \frac{16.31}{1 + exp(-0.05(V + 19.67))} \tag{6}$$

$$\alpha_h(V) = \begin{cases} 0.07 + \frac{0.11}{1+exp(0.2495(V+53.01))} & \text{if } V \leq -32.00 \\ 0.07 - \frac{0.06}{1+exp(-0.07(V-6.73))} & \text{if } V > -32.00 \end{cases} \tag{7}$$

$$\beta_h(V) = -4.8 + \frac{145.1}{1 + exp(-0.013(V - 179))} \tag{8}$$

$$\beta_m(V) = \begin{cases} 9.92 - \frac{4.575}{1+exp(-73.73(V+63.78))} & \text{if } V \leq -60.28 \\ 2.32 + \frac{2.512}{1+exp(0.2173(V+50.69))} & \text{if } -60.28 < V \leq -33.04 \\ 2.26 + \frac{1.63}{1+exp(-0.2(V+20.72))} & \text{if } -33.04 < V \leq -1.823 \\ -2.57 + \frac{6.73}{1+exp(0.07(V-40.23))} & \text{if } V > -1.823 \end{cases} \tag{9}$$

Empirical Validation of the reduced model M_H

The 13-state model M_I was substituted by M_H in the IMW model. The modified IMW model was simulated in FORTRAN. This modified model used M_H to produce the sodium current I_{Na}. Both supra and sub-threshold stimuli, lasting for 0.5ms, were used to excite the cardiac cell. S1 and S2 denote supra-threshold stimuli of -100 pA/pF and -120 pA/pF respectively. S3 and S4 denote sub-threshold stimuli of -10 pA/pF and -20 pA/pF.

The results plotted in Fig. 7 show the behavioral equivalence of M_H and M_I. The model retains both normal and anomalous cell-level behaviors on replacing the 13-state sodium-channel component with the 2-state abstraction within the complete cell model.

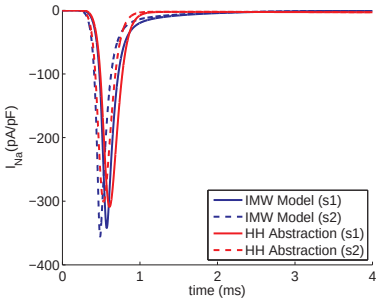

(a) Comparison of I_{Na} during the upstroke phase.

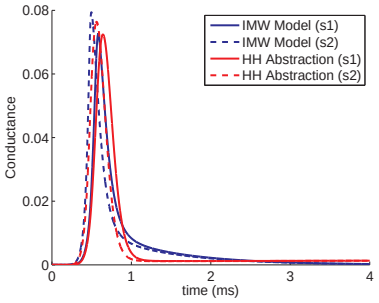

(b) Comparison of conductances $(O_1 + O_2)$ of the 13-state model M_I and (m^3h) of the 2-state abstraction M_H during the upstroke phase.

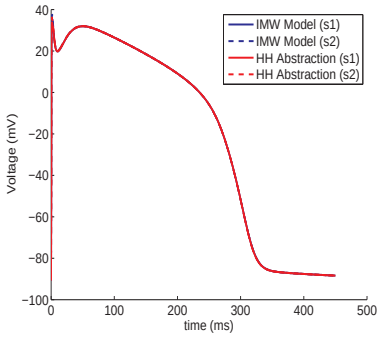

(c) Comparison of AP produced by the original IMW model and the modified version for supra-threshold stimuli.

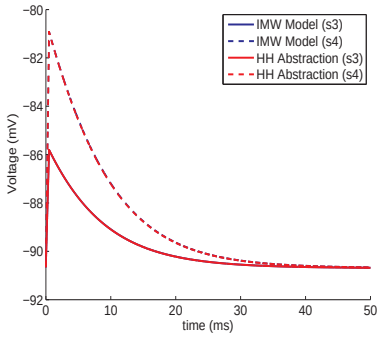

(d) Comparison of AP produced by the original IMW model and the modified version for sub-threshold stimuli.

Fig. 7. Comparison of M_I and M_H when used for I_{Na} in the IMW model. We do not show the currents and conductances for sub-threshold stimuli as they are negligible. Mean L2 errors over the duration of an AP for all stimuli: Conductance: 3.2×10^{-5}, Current: 0.1249 pA/pF, V: 0.12mV.

4 Approximate Bisimulation Equivalence of I and H

PEFT and RFI help us obtain M_H, the two-state HH-type abstraction of the 13-state model for sodium-channel dynamics M_I. We formalize the discrete-time equivalence of M_H and M_I using approximate bisimulation [15]. This notion of equivalence is stronger than the conventional behavioral equivalence, which compares the observed behaviors (trajectories) of two systems.

Moreover, the approximate bisimulation relation between the state-spaces of the systems can be utilized for gaining physiological insights from formal analysis. Analysis can be done on the abstract model M_H and the results can be interpreted in the state-space of the physiological model M_I.

In [15], Pappas et al. define approximate bisimulation equivalence of Labeled Transition Systems (LTS), a generic modeling framework. We cast the models M_H and M_I as LTS and prove approximate bisimulation equivalence of their discrete-time versions. First we will establish stability properties of M_{I^v}. We use V_{res} and V_{max} to denote the resting potential and maximum potential attained at the end of the upstroke (UP) phase.

Definition 2. *A $m \times m$ square matrix M is called a closed compartmental matrix if the the following two properties are satisfied:*

1. $M_{ij} \geq 0$ *for* $i \neq j$ *- Non-diagonal entries are non-negative.*
2. $\sum_{j=1}^{n} M_{ji} = 0, \quad 1 \leq i \leq m$ *- sum of the entries in each column is 0.*

Compartmental matrices have been used to model a wide variety of systems including ones derived by applying the law of mass action to a set of monomolecular reactions [22]. A closed compartmental system is obtained when the degradation-rates of all the species is 0.

Lemma 1. *Let A^v be the constant matrix obtained by fixing $V = v$ in Eq. (3), where $v \in [V_{res}, V_{max}]$, the range swept by the AP during the upstroke (UP) phase. A^v is a closed compartmental matrix for all $v \in [V_{res}, V_{max}]$.*

Proof. All transition rates $k_{ji}(V)$, from Table 1 have the form $ae^{(bV+c)}$, where $a > 0$. Thus condition 1 of Definition 2 is satisfied by construction.

For every column i, for $i \neq j$, A_{ji} is to the outgoing transition rate from state i to state j: $k_{ji}(V)$. The diagonal entry in the i^{th} column is the negated sum of all these outgoing rates, i.e. $-\sum_{i \neq j} k_{ji}$. Thus, the second condition is also satisfied by A^v, $V_{res} \leq v \leq V_{max}$. □

Lemma 2. *The Matrix A^v, obtained by fixing $V = v$, is irreducible for all possible voltage values: $v \in [V_{res}, V_{max}]$*

Proof. A graph-theoretic proof can be made by first inducing a graph from the matrix A^v. Let $G^v(N, E)$ be the graph such that there is a node in the graph for each of the 13 states in the stochastic model in Fig. 5 and an edge $(n_i, n_j) \in E$ if and only if $A^v_{ij} \neq 0$.

Proving that G^v remains connected at all values of V, amounts to proving irreducibility of A^v. This is indeed true because of the exponential functions in Table 1. The graph G^v remains unchanged for all values $v \in [V_{res}, V_{max}]$ and is connected in that range. □

Theorem 1. *The system of differential of equations in Eq. (3) has a stable equilibrium at a fixed voltage $V = v$, where $v \in [V_{res}, V_{max}]$.*

Proof. This follows from Proposition 4 in [22]. The prerequisites for the result are:

1. The matrix A^v must be a closed compartmental matrix.
2. The entries in A^v must be constant.
3. The matrix A^v must be irreducible.

The first condition was proved in lemma 1. The second condition holds because the rates in Table 1 are either constants or functions of V. We proved the third prerequisite in Lemma 2.

Proposition 4 in [22] proves that the real part of all eigenvalues of A^v is non-positive. This guarantees stability of the equilibrium. Note that A^v may not be Hurwitz (guaranteeing asymptotic stability). □

Theorem 1 guarantees the existence of t_S, the time taken to reach a stable steady state, for any voltage $V = v$, by M_I. We proceed to cast M_I and M_H as LTS.

Definition 3. *The LTS corresponding to M_I is the sextuple $\mathcal{I} = (X_I, \mathcal{V}, \rightarrow_I, X_I^0, \Pi_I, \langle\langle . \rangle\rangle_I)$:*

- *$X_I \subseteq \mathbb{R}^{13}$ is the set of states denoting the occupancy probabilities of the 13-state stochastic model. The ordering of the states is the same as for the vector $\mathbf{p}$ in Def. 1.*
- *$\mathcal{V}$ is a family of curves (signals) of the form $[t_0, t_0 + APD] \rightarrow \mathbb{R}$ denoting inputs to the LTS. The lower limit t_0 is the time at which the AP commences and Action Potential Duration (APD) is the time for which an AP lasts. $\mathcal{V}$ represents different temporal patterns by which the transmembrane potential V can be applied (fed back) to the model described by Eq. 3, guaranteeing a solution to the system of differential equations. In the IMW model, the pattern dictated by Eq. 1.*
- *$\rightarrow_I \subseteq X_I \times \mathcal{V} \times X_I$ is the transition relation that captures the dynamics of the model M_I. $(\mathbf{x}_I, v, \mathbf{x}_I') \in \rightarrow_I$, written as $\mathbf{x}_I \xrightarrow{v}_I \mathbf{x}_I'$, holds when there exists curves $\mathcal{V} \ni v : [0, \tau] \rightarrow \mathbb{R}$ and $\xi : [0, \tau] \rightarrow \mathbb{R}^{13}$ satisfying the system of differential equations in Eq. 3 with $\xi(0) = \mathbf{x_I}$ and $\xi(\tau) = \mathbf{x_I}'$.*
- *X_I^0, a singleton consisting of the initial condition for the stochastic model in Eq. 3, is specified in Table 4 of [21] and acts as the initial state for I.*
- *$\Pi_I \subseteq \mathbb{R}$ is the set of outputs of the LTS. This set denotes the observables from the 13-state stochastic model. The I_{Na} current depends on the occupancy probabilities of the states O_1 and O_2 in Fig. 5. The output set Π_I is the set of possible values of $O_1 + O_2$, the sum of occupancy probabilities.*
- *$\langle\langle . \rangle\rangle_I$ is the output map, that given a state $\mathbf{x}_i \in X_I$, maps it to its corresponding output [5] $\pi_6(\mathbf{x}_I) + \pi_7(\mathbf{x}_I)$, the sum of the O_1 and O_2.*

It should be noted that an input $v \in \mathcal{V}$ is a curve $v : [0, \tau] \rightarrow \mathbb{R}$ that describes both the affect of the applied voltage and also the duration of time for which it is applied. We define a LTS for the HH model below.

Definition 4. *The LTS corresponding to M_H is the sextuple $\mathcal{H} = (X_H, \mathcal{V}, \rightarrow_H, X_H^0, \Pi_H, \langle\langle . \rangle\rangle_H)$:*

- *$X_H \subseteq \mathbb{R}^2$ is the set of states denoting the values of m and h in M_H.*
- *$\mathcal{V}$, the input, is the family of curves denoting patterns of the transmembrane potential applied to the HH-type abstraction M_H. It is the same as the one in Def. 3. The curves $v \in \mathcal{V}$ guarantee solutions M_H.*

[5] $\pi_j(x)$ is the standard projection function that projects the j^{th} element from the vector x.

- $\rightarrow_H \subseteq X_H \times \mathcal{V} \times X_H$ *is the transition relation that captures the dynamics of the abstraction* M_H. $(\mathbf{x}_H, v, \mathbf{x}'_H) \in \rightarrow_H$, *written as* $\mathbf{x}_H \xrightarrow{v}_H \mathbf{x}'_H$, *holds when there exists curves* $\mathcal{V} \ni v : [0, \tau] \rightarrow \mathbb{R}$ *and* $\psi : [0, \tau] \rightarrow \mathbb{R}^2$ *satisfying the system of differential equations* $\dot{m}$ *and* $\dot{h}$ *of* M_H, *with* $\psi(0) = \mathbf{x}_H$ *and* $\psi(\tau) = \mathbf{x}'_H$.
- X_H^0 *is a singleton consisting of the initial condition identified by PEFT for* $M_{Hv_{res}}$, *and acts as the initial state.*
- $\Pi_H \subseteq \mathbb{R}$ *is the set of outputs of the LTS. This set denotes the observables from the 2-state HH-type abstraction. The* I_{Na} *current depends on the conductance* m^3h *for* M_H. *The set* Π_H *is the set of possible values of* m^3h.
- $\langle\langle . \rangle\rangle_H$ *is the output map, that given a state* $\mathbf{x}_H \in X_H$, *maps it to its corresponding output* $(\pi_1(\mathbf{x}_H))^3\pi_2(\mathbf{x}_H)$, *the conductance* m^3h.

We also provide LTS-definitions for M_I^v and M_H^v.

Definition 5. *The LTS corresponding to* M_{I^v} *is the sextuple* $\mathcal{I}^v = (X_{I^v}, T, \rightarrow_{I^v}, X^0_{I^v}, \Pi_{I^v}, \langle\langle . \rangle\rangle_{I^v})$. *The states* X_I^v, *outputs* Π_{I^v} *and output map* $\langle\langle . \rangle\rangle_{I^v}$ *is the same as Def. 3.*

- $T \subseteq \mathbb{R}_{\geq 0}$ *is the input, denoting time.*
- $\rightarrow_{I^v}$ *is the transition relation.* $\mathbf{x}_I^v \xrightarrow{t}_{I^v} \mathbf{x}_I^{v'}$ *holds if there exists a solution* ξ^v *to the linear system* (M_I^v), *satisfying* $\xi^v(0) = \mathbf{x}_I^v$ *and* $\xi^v(t) = \mathbf{x}_I^{v'}$.
- $X^0_{I^v}$ *is the initial condition obtained by simulating the system of equations in Eq. 3 in MATLAB as described in step-1 of Section 3.*

Definition 6. *The LTS corresponding to* M_{H^v} *is the sextuple* $\mathcal{H}^v = (X_{H^v}, T, \rightarrow_{H^v}, H^0_v, \Pi_{H^v}, \langle\langle . \rangle\rangle_{H^v})$. *The states* X_{H^v}, *outputs* Π_{H^v} *and output map* $\langle\langle . \rangle\rangle_{H^v}$ *is the same as Def. 4. The input set* T *is the same as Def. 5.*

- $\rightarrow_{H^v}$ *is the transition relation.* $\mathbf{x}_H^v \xrightarrow{t}_{H^v} \mathbf{x}_H^{v'}$ *holds if there exists a solution* ψ^v *to the linear system* (M_H^v), *satisfying* $\psi^v(0) = \mathbf{x}_H^v$ *and* $\psi^v(t) = \mathbf{x}_H^{v'}$.
- H_v^0 *is the initial condition determined by PEFT at* $V = v$ *as described in step-2 of Sec 3.*

Definition 7. *The two LTS* $T_1(Q_1, \Sigma, \rightarrow_1, Q_1^0, \Pi, \langle\langle . \rangle\rangle_1)$ *and* $T_2(Q_2, \Sigma, \rightarrow_2, Q_2^0, \Pi, \langle\langle . \rangle\rangle_2)$ *are approximate bisimulation equivalent, also termed approximately bisimilar, with precision* δ *(denoted as* $T_1 \cong_\delta T_2$*), if there exists a relation* $B_\delta \subseteq Q_1 \times Q_2$ *such that:*

1. *For every* $q_1 \in Q_1^0$, *there exists a* $q_2 \in Q_2^0$ *such that* $(q_1, q_2) \in B_\delta$
2. *For every* $(q_1, q_2) \in B_\delta$, $d_\Pi(\langle\langle q_1 \rangle\rangle_1, \langle\langle q_2 \rangle\rangle_2) \leq \delta$
3. *For every* $(q_1, q_2) \in B_\delta$*:*
   (a) $q_1 \xrightarrow{\sigma}_1 q_1'$, $\sigma \in \Sigma$ *implies the existence of* $q_2 \xrightarrow{\sigma}_2 q_2'$ *such that* $(q_1', q_2') \in B_\delta$.
   (b) $q_2 \xrightarrow{\sigma}_2 q_2'$, $\sigma \in \Sigma$ *implies the existence of* $q_1 \xrightarrow{\sigma}_1 q_1'$ *such that* $(q_1', q_2') \in B_\delta$.

The relation B_δ *is called the approximate bisimulation relation.*

We prove a simple lemma relating finite-length trajectories of two Linear Autonomous Dynamical Systems (LADS).

Lemma 3. *Consider two LADS* $\{\dot{\mathbf{x}}_1 = M_1.\mathbf{x}_2,\ \mathbf{x}_1(0) = \mathbf{x}_1^0\}$ *and* $\{\dot{\mathbf{x}}_2 = M_2.\mathbf{x}_2,\ \mathbf{x}_2(0) = \mathbf{x}_2^0\}$ *where* $\mathbf{x}_1, \mathbf{x}_2, \mathbf{x}_1^0, \mathbf{x}_2^0 \in \mathbb{R}^n$ *and* M_1 *and* M_2 *are* $n \times n$ *matrices. Let* $\mathbf{x}_1(t)$ *and* $\mathbf{x}_2(t)$ *be the respective solution trajectories. Let* $I_1[t_1, t_2]$ *and* $I_2[t_2, t_3]$ *be two time-intervals of arbitrary lengths such that:*

- $|\mathbf{x}_1(t) - \mathbf{x}_2(t)| \leq \delta$ *for* $t \in I_1$.
- $|\mathbf{x}_1(t) - \mathbf{x}_2(t)| \leq \delta$ *for* $t \in I_2$.

Then $|\mathbf{x}_1(t) - \mathbf{x}_2(t)| \leq \delta$ *for* $t \in I_{12}[t_1, t_3]$.

Proof. The proof follows from uniqueness and continuity of the trajectories in I_{12} □

Theorem 2. *Let* $\mathcal{I}^v$ *be the LTS corresponding to* M_{I^v}. *Let* $\mathcal{H}^v$ *be the LTS of* M_{H^v} *identified by PEFT. Then PEFT can ensure that* $I^v \cong_{\delta^v} H^v$ *for any* $v \in [V_{res}, V_{max}]$. *The precision* δ^v *is the maximum L2 error incurred by the optimizer while solving Eq. (4).*

Proof. The approximate bisimulation relation $B_{\delta^v} \subseteq X_{I^v} \times X_{H^v}$ can be constructed as follows.

1. The initial condition in $\mathbf{x}_{I^v}^0 \in X_{I^v}^0$ is paired with the initial condition $\mathbf{x}_{H^v}^0 \in X_{H^v}^0$.
2. Consider a state $\mathbf{x}_{I^v} \in X_{I^v}$ such that $\mathbf{x}_{I^v}^0 \xrightarrow{t}_{I^v} \mathbf{x}_{I^v}$, $t \in T$. Also say $\mathbf{x}_{H^v} \in X_{H^v}$ such that $\mathbf{x}_{H^v}^0 \xrightarrow{t}_{H^v} \mathbf{x}_{H^v}$. Then, $(\mathbf{x}_{I^v}, \mathbf{x}_{H^v}) \in B_{\delta^v}$. The existence of states $\mathbf{x}_{I^v}$ and $\mathbf{x}_{H^v}$ satisfying the conditions is guaranteed due to uniqueness and existence of solutions to LADS.

The relation B_{δ^v} is a valid approximate bisimulation relation:

1. The relation B_{δ^v} satisfies condition 1 in Def. 7 by construction.
2. Consider the pair $(\mathbf{x}_{I^v}, \mathbf{x}_{H^v}) \in B_{\delta^v}$. The construction of B_{δ^v} and uniqueness and existence of the solutions to M_I^v and M_H^v ensure that if $\mathbf{x}_{I^v}^0 \xrightarrow{t}_{I^v} \mathbf{x}_{I^v}$, then $\mathbf{x}_{H^v}^0 \xrightarrow{t}_{H^v} \mathbf{x}_{H^v}$. Depending on t, the time taken to evolve to $\mathbf{x}_{I^v}$ or $\mathbf{x}_{H^v}$ from the initial state, two cases arise:
   - **Case 1:** $t \leq t_S$, the time taken to reach steady state
     PEFT ensures that $\langle\langle \mathbf{x}_{I^v} \rangle\rangle_{I^v} - \langle\langle \mathbf{x}_{H^v} \rangle\rangle_{H^v}$ is bounded [6]. The bound δ^v is the worst-case L2 error incurred while solving Eq. (4).
   - **Case 2:** $t > t_S$
     $\langle\langle \mathbf{x}_{I^v} \rangle\rangle_{I^v} - \langle\langle \mathbf{x}_{H^v} \rangle\rangle_{H^v}$ is still bounded by δ^v because the output does not change after the steady state is reached. A stable steady state is guaranteed by Theorem 1 for any $v \in [V_{res}, V_{max}]$.

   This proves that condition 2 in Def. 7 is satisfied.
3. Step 3 of constructing B_{δ^v} ensures that condition 3 of Def. 7 is also satisfied, due to Lemma 3. □

We now define perturbed LADS. Then we prove the discrete-time approximate bisimilarity of M_H, the 2-state abstraction identified by the procedure described in Sec. 3, and M_I the 13-state stochastic model of sodium-channel dynamics.

[6] Lipschitz continuity of the solution-trajectories is assumed. This is needed to port the result from the discrete-time bound obtained by PEFT to continuous-time.

Definition 8. *Consider a LADS* $\{\dot{\mathbf{x}} = M.\mathbf{x},\ \mathbf{x}(0) = \mathbf{x}^0\}$*, where* $\mathbf{x} \in \mathbb{R}^n$*,* M *is a* $n \times n$ *matrix and* $\mathbf{x}(0)$ *is the initial condition. An* ϵ*-perturbation of the LADS is obtained by perturbing any of the entries in* M *or* $\mathbf{x}(0)$ *by at-most* $\epsilon \in \mathbb{R}$*.*

Theorem 3. *In discrete-time ,* $\mathcal{H}_d \cong_\delta \mathcal{I}_d$*, where* $\mathcal{H}_d$ *is the discrete-time LTS corresponding to* M_H*, and* $\mathcal{I}_d$ *is the discrete-time LTS corresponding to* M_I*. The precision* $\delta \leq 7.58 \times 10^{-4}$*.*

Proof. The discrete-time LTS $\mathcal{H}_d$ and $\mathcal{I}_d$ are similar to $\mathcal{H}$ and $\mathcal{I}$ in Def. 4 and Def. 3 respectively, with the following differences:

- The input curves v are discrete-time signals of voltage of the the form $[v_1, v_2, \ldots, v_i, \ldots]$, where v_i is the voltage at the i^{th} discrete-time step.
- The transition relation of $\mathcal{H}_d$ follows the dynamics of M_H^v but in discrete-time. Similarly, the transition relation of $\mathcal{I}_d$ follows Eq. (3) in discrete time. Chapter 11 of [27] provides details about converting continuous-time models to discrete-time version via techniques like sample and hold.

In discrete-time, the evolution of the abstraction M_H can be modeled as a series of one-step evolutions of M_{H^v}. For example, when the input signal is of the form $[v_1, \ldots, v_i, v_{i+1} \ldots]$, at the i^{th} time-step, the LADS $M_{H^{v_i}}$ evolves for one time-step, followed by $M_{H^{v_{i+1}}}$ and so on. This idea is also illustrated in Fig. 4(b).

For an arbitrary input signal $v = [v_1, \ldots, v_i, \ldots]$, at the i^{th} time-step, the LADS $M_{H^{v_i}}$ is an ϵ-perturbation of $M_{H^{v_i^*}}$, where v_i^* is a voltage-value that was processed by PEFT, i.e a trajectory of $M_{I^{v_i^*}}$ was matched by estimating the parameters of $M_{H^{v_i^*}}$. We bound the perturbation ϵ as follows:

$\epsilon = max(\epsilon_1, \epsilon_2)$ where,

$$\epsilon_1 = \max_{1 \leq j \leq n} [max\{|\alpha_m(v_j) - \alpha_m(v_{j+1})|, |\beta_m(v_j) - \beta_m(v_{j+1})|, |\alpha_h(v_j) - \alpha_h(v_{j+1})|, |\beta_h(v_j) - \beta_h(v_{j+1})|\}]$$

$$\epsilon_2 = max[|\alpha_m(v_\Delta) - \alpha_m(v_{\Delta+1})|, |\beta_m(v_\Delta) - \beta_m(v_{\Delta+1})|, |\alpha_h(v_\Delta) - \alpha_h(v_{\Delta+1})|, |\beta_h(v_\Delta) - \beta_h(v_{\Delta+1})|]$$

$$\Delta = \operatorname*{argmax}_{1 \leq j \leq n} [\tfrac{|v_j - v_{j+1}|}{2}]$$

The limit n is the total number of voltage-values processed by PEFT (also the size of the parameter-table τ and the set of finite-length behaviors $\mathcal{B}^*$). The rate-functions $\alpha_m(V)$, $\beta_m(V)$, $\alpha_h(V)$, $\beta_h(V)$ were found by the RFI procedure. The term ϵ_1 accounts for sharp changes in these functions. On the other hand, ϵ_2 accounts for sparsity in the voltage-values observed in the UP phase. Given the input signal v, the i^{th} step v_i may be at most Δ mV away from a voltage-value processed by PEFT.

It should be noted that ϵ provides a bound for the perturbation of $M_{H^{v_i}}$ wrt the "closest" $M_{H^{v_i^*}}$, i.e. at the i^{th} time-step, the perturbation is the least for $M_{H^{v_i^*}}$ among all the other voltage-values that were processed by PEFT. As the input signal v changes, this closest-system changes. At the i^{th} step, let

$M_{H^{v_i}}$ be an ϵ-perturbation of $M_{H^{v_i^*}}$ and at the $(i+1)^{th}$ step, let $M_{H^{v_{i+1}}}$ be an ϵ-perturbation of $M_{H^{v_{i+1}^*}}$. We can always ensure that $v_i^* \neq v_{i+1}^*$. This can be done by first bounding the time-scale, which determines the maximum rate-of-change of the membrane potential ($|v_i - v_{i+1}|$). Once we know the least value of $|v_i - v_{i+1}|$, we can perform the PEFT procedure for voltage-values that satisfy $\Delta \leq |v_i - v_{i+1}|$.

Using the above-mentioned approach, we ensure that at the i^{th} step, the perturbed-system $M_{H^{v_i}}$ diverges from $M_{H^{v_i^*}}$ for at most one time-step. We now bound the one-step divergence between the trajectories of $M_{H^{v_i}}$ and $M_{H^{v_i^*}}$. The system $M_{H^{v_i^*}}$ at $V = v_i^*$, consists of uncoupled differential equations for the state variables m and h. We calculate the sensitivity of the variable m to an ϵ-change in the parameters and the initial conditions below.

$$\begin{aligned}
\dot{m}^{v_i^*} &= \alpha_m^{v_i^*}(1-m) + \beta_m^{v_i^*} m \\
m^{v_i^*}[1] &= m_0^{v_i^*} + [\alpha_m^{v_i^*}(1 - m_0^{v_i^*}) + \beta_m^{v_i^*} m_0^{v_i^*}] \quad \text{(in discrete-time)} \\
m^{v_i}[1] &= m_0^{v_i^*} + \epsilon + [(\alpha_m^{v_i^*} + \epsilon)(1 - m_0^{v_i^*}) + (\beta_m^{v_i^*} + \epsilon) m_0^{v_i^*}] \text{(perturbed)} \\
|m^{v_i^*}[1] - m^{v_i}[1]| &= |\epsilon[1 + (1 - 2m - \alpha_m^{v_i} - 2\epsilon - \beta_m^{v_i})]| \quad \text{(divergence)} \\
&\leq |2\epsilon|
\end{aligned}$$

The divergence is maximized when $m = 0$ and the transition rates $\alpha, \beta = 0$. Thus given an initial separation of ϵ, the trajectories diverge by at most 2ϵ in one time-step. The same calculation can be repeated independently for h.

Theorem 2 dictates that the trajectories of $M_{I^{v_i^*}}$ and $M_{H^{v_i^*}}$ may not diverge beyond δ^{v^*}. This is implied by their approximate bisimulation equivalence.

Using a similar approach as above, we now bound the divergence of trajectories of $M_I^{v_i}$ from $M_I^{v_i^*}$, where v_i^* is determined as above. Voltage v_i^* depends upon the current state of $M_{H^{v_i}}$. At any voltage $V = v_i$, the maximum possible perturbation μ of $M_I^{v_i}$ from $M_I^{v_i^*}$, where v_i^* is the nearest voltage processed by PEFT, can be bound as was done for ϵ. The solution trajectory of $M_I^{v_i^*}$ is given by the matrix exponential $e^{A(v_i^*)t}$, where A is the matrix in Eq.(3). An arbitrary voltage v_i in the input-signal presents a μ-perturbation of $A(v_i^*)$. The evolution of $M_{I^{v_i}}$ is then approximated by the corresponding perturbation of $e^{A(v_i^*)t}$.

The matrix exponential is determined by the eigenvalues of $A(v_i^*)$. Bauer-Fike theorem [2] bounds the spectral perturbation caused due to a perturbation of the original matrix. It ensures that the eigenvalues of $A(v_i)$ are μ-perturbations of the eigenvalues of $A(v_i^*)$. Thus, the maximum divergence[7] of $M_I^{v_i}$ from $M_I^{v_i^*}$ in one time-step is at most e^{μ}.

Thus, $\delta \leq 16\epsilon^4 + \underset{1 \leq i \leq n}{\text{argmax}}[\delta^{v_i^*}] + e^{\mu}$, sum of the following quantities:

[7] A tighter bound can be found, as was done for $M_{H^{v_i}}$, by projecting the error onto the O_1 and O_2 dimensions.

– Maximum divergence of $M_{H^{v_i}}$ from $M_{H^{v_i^*}}$ over one time-step: $16\epsilon^4$. This is due to the conductance being m^3h. We bound the divergence of m and h individually at 2ϵ.
– Maximum divergence of any $M_{H^{v_i^*}}$ from $M_{I^{v_i^*}}$ over all n voltages processed during PEFT: $\underset{1\leq i\leq n}{\text{argmax}}[\delta^{v_i^*}]$. This was estimated to be 2.79×10^{-4}.
– Maximum divergence of $M_{I^{v_i}}$ from $M_{I^{v_i^*}}$ over one time-step: e^{μ}. □

5 Related Work

Various model-reduction (also known as coarse-graining) techniques have been used to reduce the simulation-time and complexity of multi-scale state-space models of chemical-reaction-kinetics [7, 18, 38]. Singular perturbation [24, 34] and invariant manifold reduction [6, 16, 17] are two such techniques. Reduction of Markovian ion-channel models, which is the central topic of this paper, has been explored in [41, 42]. The emphasis of the papers is on reducing simulation time, rather than obtaining a formal reduction. In [39] Smith et al. reduce a stochastic model for the sodium-potassium pump by lumping the states of their model. In [10], Fink et al. use mixed formulations of a HH-type model and a Markovian model to reduce the number of state variables for the calcium current.

In this paper, we provide a systematic reduction of the sodium channel responsible for the crucial upstroke phase of an AP. Conventional approaches like [25] use behavioral equivalence to validate the reduced models. Approximate bisimulation, used in this paper, formalize equivalence in a compositional setting and also help in insightful analysis. Formal reduction of the sodium-channel helps us build a *tower of abstraction* [23, 11] for the sodium-channel.

6 Conclusions and Future Work

We constructed a two-state Hodgkin-Huxley-type model M_H that can replace the 13-state continuous-time MDP model M_I for sodium-channel dynamics, in the context of the IMW cardiac-cell model.

The reduction was formalized by proving the abstract and the concrete models to be approximately bisimilar. This notion of system-equivalence can be used for compostional reasoning. When $\mathcal{H}$ is appropriately composed with rest of the larger whole-cell IMW model, approximate bisimulation guarantees that the overall composed-system retains the properties of the original system. The original system can be modeled as an appropriate composition of $\mathcal{I}$ and rest of the IMW model. In the future, further complicated non-deterministic models will be explored and reduced. Tighter bounds will also be pursued for the precision of the bisimulation relation. We then plan to use the *towers of abstraction*, constructed by the strategy outlined in the paper, for insightful analysis of cardiac models.

References

1. E. Bartocci, E. Cherry, J. Glimm, R. Grosu, S. A. Smolka, and F. Fenton. Toward real-time simulation of cardiac dynamics. In *Proceedings of the 9th International Conference on Computational Methods in Systems Biology, CMSB'2011*, pages 103–112. ACM, 2011.
2. F. L. Bauer and C. T. Fike. *Norms and Exclusion Theorems*. Numerische Matematik, 1960.
3. G. W. Beeler and H. Reuter. Sodium channels and gating currents. *Journal of Physiology*, 268:177–210, 1977.
4. A. Bueno-Orovio, M. E. Cherry, and F. H. Fenton. Minimal model for human ventricular action potentials in tissue. *J. of Theor. Biology*, 253(3):544–560, 2008.
5. E. M. Cherry and F. H. Fenton. Visualization of spiral and scroll waves in simulated and experimental cardiac tissue. *New Journal of Physics*, 10:125016, 2008.
6. E. Chiavazzo, A. N. Gorban, and I. V. Karlin. Comparisons of invariant manifolds for model reduction in chemical kinetics. *Comm Comp Phys*, 2:964 –992, 2007.
7. I. R. Epstein and J. A. Pojman. *An Introduction to Nonlinear Chemical Dynamics*. Oxford University Press, London, 1998.
8. F. Fenton and A. Karma. Vortex dynamics in three-dimensional continuous myocardium with fiber rotation: Filament instability and fibrillation. *Chaos*, 8(1):20–47, 1998.
9. F. H. Fenton and E. M. Cherry. Models of cardiac cell. *Scholarpedia*, 3:1868, 2008.
10. M. Fink and D. Noble. Markov models for ion channels: Versatility versus identifiability and speed. *Philosophical Transactions of the Royal Society A: Mathematical, Physical and Engineering Sciences*, 367(1896):2161–2179, 2009.
11. J. Fisher, N. Piterman, and M. Y. Vardi. The only way is up. In *Proceedings of the 17th international conference on Formal methods*, FM'11, pages 3–11, Berlin, Heidelberg, 2011. Springer-Verlag.
12. A. Girard. Controller synthesis for safety and reachability via approximate bisimulation. *Automatica*, 48:947–953, 2012.
13. A. Girard and G. J. Pappas. Approximate bisimulations for nonlinear dynamical systems. In *Proc. of CDC'05, the 44th Int. Conf. on Decsion and Control*, Seville, Spain, December 2005. IEEE.
14. A. Girard and G. J. Pappas. Approximate bisimulation relations for constrained linear systems. *Automatica*, 43:1307–1317, 2007.
15. A. Girard and G. J. Pappas. Approximation metrics for discrete and continuous systems. *Automatic Control, IEEE Transactions on*, 52(5):782 –798, may 2007.
16. A. N. Gorban and I. V. Karlin. Method of invariant manifold for chemical kinetics. *Chem Eng Sci*, 58:4751 –4768, 2003.
17. A. N. Gorban and I. V. Karlin. *Invariant manifolds for physical and chemical kinetics (Lecture Notes in Physics)*. Springer, 2005.
18. A. N. Gorban, N. Kazantzis, I. G. Kevrekidis, H. C. Ottinger, and C. Theodoropoulos. *Model Reduction and Coarse-Graining Approaches for Multiscale Phenomena*. Springer, 2006.
19. R. Grosu, G. Batt, F. Fenton, J. Glimm, C. L. Guernic, S. A. Smolka, and E. Bartocci. From cardiac cells to genetic regulatory networks. In *Proc. of CAV'11, the 23rd International Conference on Computer Aided Verification*, LNCS, Cliff Lodge, Snowbird, Utah, USA, July 2011. Springer.
20. A. L. Hodgkin and A. F. Huxley. A quantitative description of membrane current and its application to conduction and excitation in nerve. *Journal of Physiology*, 117:500–544, 1952.

21. V. Iyer, R. Mazhari, and R. L. Winslow. A computational model of the human leftventricular epicardial myocytes. *Biophysical Journal*, 87(3):1507–1525, 2004.
22. T. Jahnke and W. Huisinga. Solving the chemical master equation for monomolecular reaction systems analytically. *Journal of Mathematical Biology*, 54:1–26, July 2007.
23. D. H. Jasmin Fisher and T. A. Henzinger. Biology as reactivity. *Communications of the ACM*, 54(10):72–82, October 2011.
24. J. Kevorkian and J. D. Cole. *Multiple Scale and Singular Perturbation Methods*. Springer-Verlag, 1996.
25. P. Kienker. Equivalence of aggregated markov models of ion-channel gating. *Proceedings of the Royal Society of London. B. Biological Sciences*, 236(1284):269–309, 1989.
26. C.-C. Kuo and B. P. Bean. Na channels must deactivate to recover from inactivation. *Neuron*, 12:819–829, 1994.
27. E. Lee and P. Varaiya. *Structure and Interpretation of Signals and Systems*. Pearson Education, 2003.
28. M. S. J. Lisa A. Irvine and R. L. Winslow. Cardiac sodium channel markov model with tempretature dependence and recovery from inactivation. *Biophysical Journal*, 76:1868–1885, 1999.
29. C. H. Luo and Y. Rudy. A dynamic model of the cardiac ventricular action potential. I. Simulations of ionic currents and concentration changes. *Circulation Research*, 74(6):1071–1096, June 1994.
30. MATLAB. Choosing a solver. http://www.mathworks.com/help/toolbox/optim.
31. MATLAB. Curve fitting toolbox. http://http://www.mathworks.com/products /curvefitting.
32. MATLAB. Nonlinear numerical methods. http://www.mathworks.com/help/techdoc /ref/f16-5872.html.
33. MATLAB. Optimization toolbox. http://www.mathworks.com/help/toolbox/optim.
34. J. D. Murray. *Mathematical Biology*. Springer-Verlag, 1990.
35. C. J. Myers. *Engineering Genetic Circuits*. CRC Press, 2010.
36. National Science Foundation (NSF). Computational modeling and analysis of complex systems (CMACS). http://cmacs.cmu.edu.
37. D. Noble. A modification of the hodgkin-huxley equations applicable to purkinje fibre action and pace-maker potentials. *J. Physiol.*, 160:317–352, 1962.
38. O. Radulescu, A. N. Gorban, A. Zinovyev, and A. Lilienbaum. Robust simplifications of multiscale biochemical networks. *BMC Systems Biology*, 2(1):86, 2008.
39. N. Smith and E. Crampin. Development of models of active ion transport for whole-cell modelling: Cardiac sodium-potassium pump as a case study. *Progress in Biophysics and Molecular Biology*, 85(23):387 – 405, 2004. ¡ce:title¿Modelling Cellular and Tissue Function¡/ce:title¿.
40. K. H. Ten Tusscher, D. Noble, P. J. Noble, and A. V. Panfilov. A model for human ventricular tissue. *American Journal of Physiology*, 286:H1573–H1589, 2004.
41. C. Wang, P. Beyerlein, H. Pospisil, A. Krause, C. Nugent, and W. Dubitzk. An efficient method for modeling kinetic behavior of channel proteins in cardiomyocytes. *IEEE/ACM Trans. on Computational Biology and Bioinformatics*, 9(1):40–51, Jan/Feb 2012.
42. J. P. Whiteley. Model reduction using a posteriori analysis. *Mathematical Biosciences*, 225(1):44 – 52, 2010.

Qualifications for the student paper award

1. **Lead author's affiliation**: Abhishek Murthy, PhD student, Department of Computer Science, Stony Brook University.
2. **Contributions of various authors** The key contributions of our paper are:
   1. Model reduction by identifying appropriate abstraction.
   2. Proving approximate bisimulation relation between the abstract and the concrete model.

   Methodology for model reduction:
   All the authors of the paper met once every week over the last few months to discuss the problem and finally came up with the correct abstractions for reducing the the 13-state model for the sodium channel of the IMW model for human ventricular epicardial myocyte. Co-authors Flavio Fenton and Elizabeth Cherry were consulted for biological insights. Co-authors James Glimm and Ezio Bartocci were consulted for implementation of the PEFT and RFI routines.
   Implementation of the Methodology: Done completely by Md. Ariful Islam and Abhishek Murthy under the guidance of Prof. Grosu and Prof. Smolka.
   Proving approx bisimulation relation: Formulating the lemmas, theorems and their proofs was jointly done by Abhishek Murthy and Md. Ariful Islam under the guidance of Prof. Grosu and Prof. Smolka.
   FORTRAN code for IMW model simulation Co-author Elizabeth Cherry provided the FORTRAN code for the simulation of the IMW model.